Circulation

ORIGINAL RESEARCH ARTICLE

4HNE Impairs Myocardial Bioenergetics in Congenital Heart Disease-Induced Right Ventricular Failure

HyunTae V. Hwang, PhD
Nefthi Sandeep, MD
Sharon L. Paige, MD, PhD
Sara Ranjbarvaziri, PhD
Dong-Qing Hu, MD
Mingming Zhao, MD
Ingrid S. Lan, MS
Michael Coronado, PhD
Kristina B. Kooiker, PhD
Sean M. Wu, MD, PhD
Giovanni Fajardo, MD
Daniel Bernstein, MD
Sushma Reddy, MD

BACKGROUND: In patients with complex congenital heart disease, such as those with tetralogy of Fallot, the right ventricle (RV) is subject to pressure overload stress, leading to RV hypertrophy and eventually RV failure. The role of lipid peroxidation, a potent form of oxidative stress, in mediating RV hypertrophy and failure in congenital heart disease is unknown.

METHODS: Lipid peroxidation and mitochondrial function and structure were assessed in right ventricle (RV) myocardium collected from patients with RV hypertrophy with normal RV systolic function (RV fractional area change, 47.3±3.8%) and in patients with RV failure showing decreased RV systolic function (RV fractional area change, 26.6±3.1%). The mechanism of the effect of lipid peroxidation, mediated by 4-hydroxynonenal ([4HNE] a byproduct of lipid peroxidation) on mitochondrial function and structure was assessed in HL1 murine cardiomyocytes and human induced pluripotent stem cell-derived cardiomyocytes.

RESULTS: RV failure was characterized by an increase in 4HNE adduction of metabolic and mitochondrial proteins (16 of 27 identified proteins), in particular electron transport chain proteins. Sarcomeric (myosin) and cytoskeletal proteins (desmin, tubulin) also underwent 4HNE adduction. RV failure showed lower oxidative phosphorylation (moderate RV hypertrophy, 287.6±19.75 versus RV failure, 137.8±11.57 pmol/[sec×mL]; P=0.0004), and mitochondrial structural damage. Using a cell model, we show that 4HNE decreases cell number and oxidative phosphorylation (control, 388.1±23.54 versus 4HNE, 143.7±11.64 pmol/[sec×mL]; P<0.0001). Carvedilol, a known antioxidant did not decrease 4HNE adduction of metabolic and mitochondrial proteins and did not improve oxidative phosphorylation.

CONCLUSIONS: Metabolic, mitochondrial, sarcomeric, and cytoskeletal proteins are susceptible to 4HNE-adduction in patients with RV failure. 4HNE decreases mitochondrial oxygen consumption by inhibiting electron transport chain complexes. Carvedilol did not improve the 4HNE-mediated decrease in oxygen consumption. Strategies to decrease lipid peroxidation could improve mitochondrial energy generation and cardiomyocyte survival and improve RV failure in patients with congenital heart disease.

Key Words: heart failure ■ heart ventricles ■ hypertrophy ■ lipid peroxidation ■ mitochondria

Sources of Funding, see page 1681

https://www.ahajournals.org/journal/circ

Clinical Perspective

What Is New?

- We show that right ventricular failure is characterized by increased oxidation of membrane phospholipids, known as lipid peroxidation and its products such as 4-hydroxynonenal (4HNE).
- 4HNE binds to metabolic and mitochondrial proteins and was associated with decreased myocardial energy generation and mitochondrial structural disruption with increasing severity of right ventricular hypertrophy and right ventricular failure.
- Mechanistically, we show that 4HNE is sufficient to decrease energy generation by inhibiting electron transport chain complex activities and mitochondrial dynamics.

What Are the Clinical Implications?

- The mechanisms of congenital heart disease-associated right ventricular dysfunction are not well known, limiting the availability of therapeutic approaches.
- Since standard heart failure therapies such as angiotensin-converting enzyme inhibitors and beta blockers are ineffective in the treatment of right ventricle failure, developing therapies focusing on new targets such as lipid peroxidation could improve right ventricular function in congenital heart diseases by improving mitochondrial energy generation and cardiomyocyte survival.

Children with complex congenital heart disease involving right-sided obstructive lesions such as tetralogy of Fallot, pulmonary atresia/intact ventricular septum, and hypoplastic left heart syndrome or pulmonary hypertension are at risk for right ventricular (RV) failure and decreased survival.[1–3] However, the incidence and timing of RV failure varies,[2,4] and current noninvasive and invasive diagnostic modalities can neither predict which patients will progress to RV failure nor detect the preceding subclinical changes occurring on the molecular and cellular level. In addition, standard heart failure therapies such as angiotensin-converting enzyme inhibitors and β blockers are ineffective in the treatment of RV failure.[5]

We focused on the critical role of oxidative stress on mitochondrial bioenergetics during RV hypertrophy and the progression to RV failure in congenital heart disease involving right-sided obstructive lesions. The human heart is a highly oxidative organ cycling a daily amount of ATP (adenosine triphosphate) up to 15 to 20 times its own weight,[6] and is thus particularly vulnerable to oxidative damage. Oxidation of membrane phospholipids, known as lipid peroxidation, is the most prominent manifestation of oxidative stress in the heart in aging and in ischemia/reperfusion injury, and is uniformly detrimental to cardiac function.[7–9] However, little is known about the role of lipid peroxidation and individual lipid peroxidation products such as the potent reactive aldehyde 4-hydroxynonenal (4HNE) in RV hypertrophy and failure. 4HNE is of particular interest because of its ability to adduct or modify proteins by covalent bonding, thereby inhibiting or altering their function.[10,11] Because mitochondria are the largest source and target of lipid peroxidation,[12] we hypothesized that 4HNE adversely affects mitochondrial energy generation in RV pressure overload, leading to impaired cardiac function and RV failure. Carvedilol, a known antioxidant, has been shown to decrease lipid peroxidation of mitochondrial membranes in ischemic heart disease[13] and to decrease 4HNE expression in dilated cardiomyopathy,[14] and was therefore investigated as a candidate drug to rescue lipid peroxidation-induced mitochondrial dysfunction. An improved understanding of the effect of lipid peroxidation on the complex processes of oxidative stress and mitochondrial function could aid in developing novel diagnostic tools for monitoring the progression of the vulnerable RV to failure and for therapeutics to delay the onset of RV failure and improve the quality of life in patients with congenital heart disease.

METHODS

The data that support the findings of this study are available from the corresponding author on reasonable request.

RV Myocardial Samples from Patients With Right Ventricular Outflow Tract Obstruction

RV muscle bundles routinely resected at the time of cardiac surgery were collected from 16 patients with RV pressure overload because of pulmonary stenosis, double-chambered RV, or tetralogy of Fallot. Patients were divided into 3 groups based on qualitative echocardiographic assessment of the degree of hypertrophy by the reading cardiologist: (1) mild RV hypertrophy (n=3); (2) moderate RV hypertrophy (n=10); and (3) severe RV hypertrophy (n=3). All patients had RV outflow tract gradients >55 mm Hg. RV systolic function measured by RV fractional area change (RV FAC) was normal in all 16 patients. These groups were compared with RV samples from 5 patients with RV pressure overload with pulmonary hypertension secondary to congenital heart disease (repaired atrioventricular septal defect, n=4; Shone complex, n=1). These patients had clinical and echocardiographic evidence of RV failure with decreased RV FAC (Table 1), necessitating heart transplantation. It was not possible to obtain healthy, nonhypertrophied RV tissue. RV muscle bundles from mild, moderate, and severe RV hypertrophy being resected by the surgeon during cardiac surgery were collected immediately on resection by the investigator's team who is on standby in the operating room. For RV failure patients, RV myocardium was resected as soon as the heart was explanted from the patient. Of this freshly resected RV tissue, 5 mg was minced and oxygen consumption was assessed immediately. Biochemical

Table 1. Patient Characteristics

	Mild RV hypertrophy	Moderate RV hypertrophy	Severe RV hypertrophy	RV failure
Number of patients	3	10	3	5
Age (years)	11.3±16.1	2.8±4.3	25.2±13.8	10.9±6.9
Sex (male)	33%	50%	33.3%	60%
Diagnoses	Pulmonary stenosis, ventricular septal defect/ double-chambered right ventricle	Tetralogy of Fallot, pulmonary stenosis, ventricular septal defect/double-chambered right ventricle	Tetralogy of Fallot, ventricular septal defect/double-chambered right ventricle	Atrioventricular septal defect, Shone complex with pulmonary hypertension
Surgical procedure	RVOT muscle bundle resection	RVOT muscle bundle resection	RVOT muscle bundle resection	Heart transplant
Peak RVOT gradient (mmHg)	57.7±2.5	82.1±18.8	119.3±19.1	51.8±32.2
RV fractional area change (%)	46±6.24	49.7±7.67	43±6.08	26.6±3.13
Left ventricular ejection fraction (%)	60±6.76	62±8.22	69±7.45	58±13.86
Medications	—	—	—	Epinephrine, dopamine, milrinone

Data are presented as mean±SD. RV tissue was collected at the time of surgical repair from patients with mild, moderate, and severe RV hypertrophy, and at the time of heart transplantation from patients with RV failure secondary to congenital heart disease. All patients with mild, moderate, and severe hypertrophy had RV pressure overload with preserved systolic function. Patients with RV pressure overload with RV failure had decreased systolic function and were on systemic inotropic therapy. RV indicates right ventricle; and RVOT, right ventricular outflow tract.

assays and electron microscopy were also evaluated based on sample availability.

Cell Culture

HL1 murine cardiomyocytes were cultured in a humidified 5% CO_2, 37 °C incubator with complete Claycomb medium (51800C; Sigma-Aldrich; St Louis, MO), following the manufacturer's guideline: 10% fetal bovine serum, 2 mM GlutaMAX (35-050-061; ThermoFisher Scientific; Waltham, MA), 100 µmol/L norepinephrine (A0937; Sigma-Aldrich), 300 nmol/L ascorbic acid (A7506; Sigma-Aldrich), and 100 U/mL penicillin-streptomycin (P4333; Sigma-Aldrich).

Protein Expression

Standard Western blot techniques for denatured and reduced samples were used. The samples were probed using the following antibodies: 4HNE, VDAC1 (voltage-dependent anion-selective channel protein 1), PGC1α (PPARG coactivator 1α), DRP1 (dynamin 1-like), MFF (mitochondrial fission factor), OPA1 (mitochondrial dynamin like GTPase), MFN2 (mitofusin 2), Enolase, and TOM20 (translocase of outer mitochondrial membrane 20). Mitochondrial fraction was isolated from HL1 cells collected by scraping, following the isolation kit's dounce-based protocol (89874; ThermoFisher Scientific). Enolase was used as the loading control for total protein and TOM20 for the mitochondrial fraction. Purity of the isolated mitochondria was assessed by confirming the absence of enolase in the mitochondrial fraction (Figure IA in the Data Supplement). We also confirmed complete removal and collection of mitochondria from the cytosolic fraction by probing for VDAC1 (Figure IB in the Data Supplement). Details of the antibodies used are shown in Table I of the Data Supplement.

Identification of 4HNE-Adducted Proteins

4HNE-adducted proteins increased in RV failure were identified by Applied Biomics (Hayward, CA). Proteins were separated using 2-dimensional gel electrophoresis in representative RV hypertrophy and RV failure patient samples (n=1/group). 4HNE-adduction levels were measured through Western blot. The 4HNE-adducted proteins were identified using mass spectrometry (matrix-assisted laser desorption/ionization-time of flight). Similarly, 4HNE adducted proteins were identified in HL1 cardiomyocytes treated with 4HNE and with 4HNE+carvedilol and compared with control.

Mitochondrial Respiration

Using a high-resolution Oxygraph2K respirometer (Oroboros Instruments; Innsbruck, Austria), we used the Chance and Williams protocol to assess oxygen consumption[15] in 5 mg of fresh, finely minced RV tissue. Nonphosphorylating oxygen consumption attributable to proton leak (leak respiration) was assessed in response to the substrates (1) malate and glutamate to evaluate complex I–nicotinamide adenine dinucleotide dehydrogenase activity, and (2) succinate to evaluate complex II–succinate dehydrogenase activity. Subsequently, oxidative phosphorylation was assessed in response to the substrate ADP to evaluate Complex V–mediated maximal respiration (state 3 respiration). Oxidative phosphorylation was calculated by subtracting complex I and II–mediated leak respiration from state 3 respiration. Respiratory control ratio was calculated by dividing state 3 respiration by complex I and II–mediated leak respiration. Nonphosphorylating state 4 leak respiration was assessed in response to oligomycin, an ATP synthase inhibitor. Uncoupled respiration was assessed in response to FCCP (carbonyl cyanide-p-trifluoromethoxyphenylhydrazone) to evaluate the maximal electron transport chain activity.[16,17] Antimycin A was used to abolish electron transport chain activity. The oxygen consumption rates are reported as O_2 flux per volume (pmol/[sec×mL]). Buffer and substrate concentrations are shown in Table II in the Data Supplement. Oxygen consumption was also assessed in HL1 cardiomyocytes (2 million cells at the time of 4HNE treatment). To further verify our results from HL1 cells, we also

measured oxygen consumption in human induced pluripotent stem cell-derived cardiomyocytes using Seahorse Analyzer (see Methods in the Data Supplement).

Our assay buffer was sufficient to allow entry of the mitochondrial substrates into the samples without other permeabilizing reagents such as saponin. This was evidenced by (1) robust oxygen consumption induced by each administered mitochondrial substrate and uncoupling reagent; and (2) similar levels of ADP-stimulated state 3 respiration to those of uncoupled respiration, which is mediated by the cell-permeable chemical FCCP. In contrast, only negligible levels of oxygen consumption were observed when the samples were suspended in PBS instead (data not shown).

Electron Microscopy

Transmission electron microscopy (JEM 1400; JEOL; Peabody, MA) was used to assess mitochondrial morphology. RV samples were fixed overnight (2% glutaraldehyde, 4% paraformaldehyde, 0.1 M sodium cacodylate, pH 7.4), treated with 1% osmium tetroxide, 1% and 3.5% uranyl acetate, and 0.2% lead citrate, sectioned and imaged. Intermyofibrillar mitochondrial number, size, morphology, network, and cristae density were analyzed by ImageJ (US National Institutes of Health; Bethesda, MD), tracing all complete mitochondrial perimeters in each image. At least 70 mitochondria per sample were assessed by an investigator blinded to the sample identity.

Mitochondrial DNA Copy Number

Mitochondrial to nuclear DNA copy number ratio was measured in RV myocardial samples. DNA was isolated from RV samples using QIA DNA Micro Kit (56304; Qiagen; Germantown, MD). Real-time quantitative PCR was performed using Human Mitochondrial Monitoring Primer Set (7246; Takara Bio; Mountain View, CA) and PowerUp SYBR Green Master mix (A25742; Applied Biosystems; Foster City, CA).

4HNE Treatment of Cardiomyocytes

HL1 cells were treated for 24 hours with 50 µmol/L of 4HNE (32100; Cayman Chemical; Ann Arbor, MI), with and without 10 µmol/L carvedilol (S1831; Selleckchem; Houston, TX). An appropriate volume of vehicles was used for other groups that were not treated with these chemicals (ethanol for 4HNE and dimethyl sulfoxide for carvedilol). After treatment, the cells were harvested to assess 4HNE adducted proteins (as previously described), oxygen consumption, mitochondrial membrane potential (tetramethylrhodamine, methyl ester; T668; ThermoFisher Scientific), fission and fusion protein expression, mitochondrial mass, and mitochondrial morphology by fluorescence imaging (MitoTracker Red CMXRos; M7512; ThermoFisher Scientific) (see Methods in the Data Supplement). All assays were performed only at 50 µmol/L 4HNE because higher doses at 100 µmol/L and 200 µmol/L were lethal to the cells at 24 hours.

Assessment of Mitochondrial Morphology

Fluorescence micrographs of mitochondria were quantified using FIJI[18] through custom macros, and 7 to 15 micrographs were analyzed per group. The micrographs were background-subtracted with rolling-ball radius of 5, followed by 10 pixels, then denoised through the Despeckle function. At each step, the signals were normalized with the Enhance Contrast function. The processed images were then thresholded to select the mitochondria, which were subsequently analyzed through the Analyze Particle function. Median values for each micrograph were used for statistical analysis.

Statistics

Student *t* test was used for comparison between 2 groups. One-way ANOVA with Tukey multiple testing correction was used for 3 or more group comparisons, and 2-way ANOVA was used for groups with 2 independent variables. For nonnormal data, Kruskal–Wallis test was used. Correlation was assessed using Pearson correlation. We performed multiple regression analysis to assess differences in oxidative phosphorylation between groups after correcting for age. All data are presented as mean±SEM and description of patient cohort is presented as mean±SD. A P value of ≤0.05 was considered significant.

Study Approval

This study was approved by the Stanford University Institutional Review Board. Consent was obtained from all patients and/or their parents; in addition, assent was obtained for those >7 years of age.

RESULTS

Patient Characteristics

RV myocardial samples were collected from patients with mild, moderate, and severe RV hypertrophy attributable to pulmonary stenosis, double-chambered RV, or tetralogy of Fallot, and compared with RV myocardial samples from patients with RV failure attributable to pulmonary hypertension secondary to repaired atrioventricular septal defect and Shone complex. RV hypertrophy was qualitatively assessed by echocardiography as mild, moderate and severe RV hypertrophy based on ventricular wall thickness. The mean age of the hypertrophy groups was 13.1±6.5 years and RV failure was 10.9±3.1 years. In the hypertrophy groups, 39% were male and in the RV failure group, 60% were male. Peak RV outflow tract gradient was >55 mm Hg in the hypertrophy groups and >50 mm Hg in RV failure. RV systolic function was normal in the RV hypertrophy groups (RV FAC, 47.3±3.8%) and decreased in RV failure (RV FAC, 26.6±3.1%). Left ventricular ejection fraction was preserved in all groups (Table 1). Patients in all categories of RV hypertrophy were on no cardiac medications, while all patients with RV failure were on systemic inotropes in the form of epinephrine, dopamine, and/or milrinone infusions.

4HNE, A Lipid Peroxidation-Induced Reactive Aldehyde, Is Increased in Patients With RV Failure

4HNE protein expression was assessed in RV samples collected from patients with mild, moderate, and severe RV hypertrophy and in patients with RV failure. The level of 4HNE protein adducts was increased in RV failure (moderate RV hypertrophy, 0.584±0.222 vs RV failure, 1.647±0.17; *P*=0.0035) (Figure 1A and 1B).

Metabolic and Mitochondrial Proteins Are Highly Susceptible to 4HNE-Adduction in RV Failure

We next assessed the identity of the proteins susceptible to 4HNE-adduction (Figure 1C through 1F; n=1/group). Twenty-seven 4HNE-adducted proteins which increased in RV failure (≥1.3-fold change) were selected for identification (Table 2). It is interesting that 16 of the 27 proteins were metabolic pathway proteins and most were directly related to mitochondrial metabolism. Several proteins involved in electron transport chain activity and mitochondrial respiration, including nicotinamide adenine dinucleotide dehydrogenase, cytochrome b, and cytochrome c were affected. Other 4HNE-adducted mitochondrial proteins include the mitochondrial elongation factor EF-Tu, which is critical for mitochondrial protein synthesis and thus can directly affect the assembly of mitochondrial components. In addition, mitochondrial proteins involved in survival and stress response were targeted by 4HNE. Mitochondrial stress-70 protein is a chaperone protein, critical for mitochondrial biogenesis and proteostasis, conferring protection against oxidative and other cytotoxic stresses. Manganese superoxide dismutase, a well-recognized mitochondrial antioxidant enzyme, converts toxic mitochondrial superoxides into less reactive hydrogen peroxide. Therefore, 4HNE adduction of metabolic and mitochondrial proteins targets electron transport chain proteins, mitochondrial protein synthesis, and prosurvival pathways.

Cardiac Structural Proteins Are Highly Susceptible to 4HNE Adduction in RV Failure

Major sarcomeric proteins (myosin) mediating cardiac contraction, as well as cytoskeletal proteins (desmin/tubulin) connecting neighboring sarcomeres together and connecting the contractile apparatus to the mitochondria, were susceptible to 4HNE adduction (Table 2). Among the most highly 4HNE-adducted proteins were (1) myoglobin, which facilitates oxygen diffusion from the capillaries to the mitochondria (3-fold); (2) cysteine and glycine-rich protein 3 (25.6-fold), a scaffold protein that promotes assembly of complexes along the sarcomere and which acts as a stretch sensor; and (3) collagen alpha-1 (6-fold), a major structural component of microfibrils known to cause t-tubule remodeling in heart failure.

Oxidative Phosphorylation and Uncoupled Respiration Are Impaired in Patients With Severe RV Hypertrophy and RV Failure

To understand the significance of the increased 4HNE-adduction to metabolic and mitochondrial proteins in RV failure, we evaluated oxygen consumption in patient myocardial tissues as a marker of mitochondrial function (Figure 2A and 2B). Complex I and II–mediated leak respiration did not change with RV hypertrophy and failure (Figure 2C and 2D). Both oxidative phosphorylation (Figure 2E) and uncoupled respiration (Figure 2F) trended toward an increase in the moderate RV hypertrophy group (with preserved RV systolic function), and decreased in the severe RV hypertrophy and RV failure groups (oxidative phosphorylation: moderate RV hypertrophy, 287.6±19.75 vs RV failure, 137.8±11.57 pmol/[sec×mL]; *P*=0.0003) (uncoupled respiration: moderate RV hypertrophy, 446.8±26.13 vs RV failure, 254.5±25.1 pmol/[sec×mL]; *P*=0.0006). The respiratory control ratio (Figure 2G) trended toward an increase in moderate hypertrophy and decreased in severe hypertrophy and RV failure (respiratory control ratio: moderate RV hypertrophy, 4.05±0.49 vs RV failure, 2.47±0.16 pmol/[sec×mL]; *P*=0.0079). The cohort of patients with end stage RV failure was too small to correlate increasing 4HNE expression with the acuity of illness, duration of heart failure, medication use, or mitochondrial respiration. We tested whether the increased oxygen consumption seen in moderate RV hypertrophy could have been influenced by the higher percent of infants in this group. Children with moderate RV hypertrophy <1 year versus >1 year of age (mean age, 0.32±0.1 vs 5.37±5.1 years) showed no difference in oxidative phosphorylation (312.9±34.41 vs 262.2±15.8; *P*=0.161) (Figure 2H). Similarly, linear regression analysis of oxidative phosphorylation and age (Figure 2I) demonstrated a low R^2 at 0.32 suggesting that although age does play a role, it is responsible for only about one-third of the variation in oxidative phosphorylation. The slope of the line representing the actual change per year in oxidative phosphorylation was very low at −4.23 pmol/(sec×mL) ($y = -4.23+260.7$; R^2=0.32, *P*=0.007), suggesting that while age does play a small role in changes in oxidative phosphorylation, the changes we describe with RV failure are greater. Similarly aged patients also had

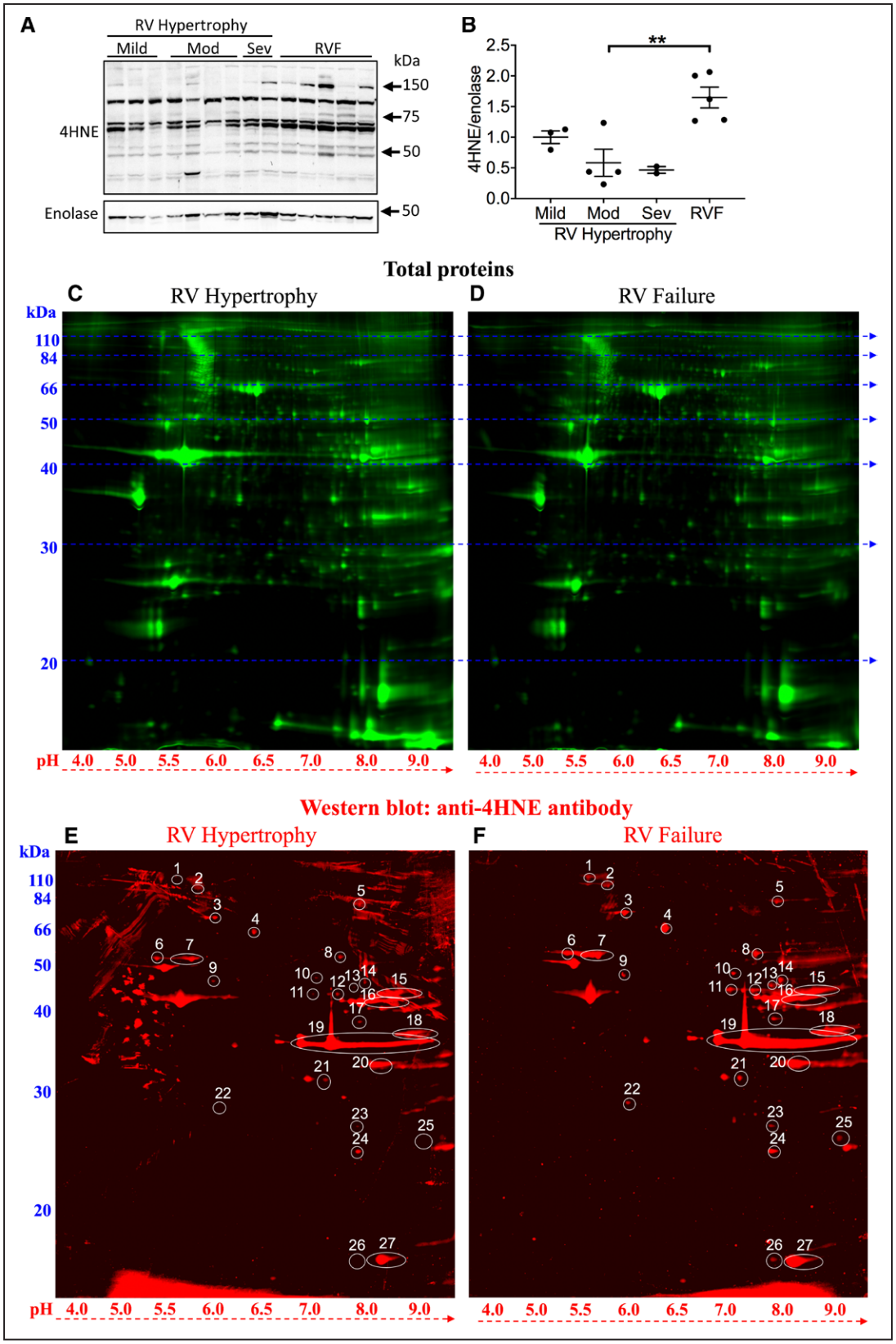

Figure 1. Lipid peroxidation is increased in RV failure.
A, B, 4HNE adducts increased with RV failure versus moderate RV hypertrophy, n=2–5 per group. **C, D**, Two-dimensional gel electrophoresis and Western blot were used to detect total protein in representative RV hypertrophy (n=1) and RV failure (n=1) samples. **E, F,** Two-dimesnional gel electrophoresis and Western blot were used to detect the proteins with increased 4HNE adducts. Twenty-seven protein spots where 4HNE signals were higher in RV failure versus RV hypertrophy were numbered for identification. 4HNE indicates 4-hydroxynonenal; Mod, moderate; RV, right ventricle; RVF, right ventricular failure; and Sev, severe. Data are presented as mean±SEM. $^{**}P<0.01$.

Table 2. 4HNE Modification of Metabolic and Mitochondrial Proteins Characterize Oxidant Stress in RV Failure

Category	Spot number	4HNE-modified protein name	Accession number	Fold change
Metabolism	22	NADH dehydrogenase [ubiquinone] iron-sulfur protein 3, mitochondrial	NDUS3_HUMAN	2.58
	11	NADH dehydrogenase [ubiquinone] iron-sulfur protein 2, mitochondrial	NDUS2_HUMAN	2.55
	12	Elongation factor Tu, mitochondrial	EFTU_HUMAN	2.53
	14	Beta-enolase	ENOB_HUMAN	2.35
	8	Dihydrolipoyl dehydrogenase, mitochondrial	DLDH_HUMAN	2.26
	16	Creatine kinase M-type	KCRM_HUMAN	2.05
	19	Malate dehydrogenase, cytoplasmic	MDHC_HUMAN	2.02
	10	Alpha-enolase	ENOA_HUMAN	1.99
	23	ES1 protein homolog, mitochondrial	ES1_HUMAN	1.88
	13	Fumarate hydratase, mitochondrial	FUMH_HUMAN	1.70
	18	Glyceraldehyde-3-phosphate dehydrogenase	G3P_HUMAN	1.69
	15	Creatine kinase S-type, mitochondrial	KCRS_HUMAN	1.68
	9	Cytochrome b-c1 complex subunit 1, mitochondrial	QCR1_HUMAN	1.66
	5	Aconitate hydratase, mitochondrial	ACON_HUMAN	1.62
	17	NADH dehydrogenase [ubiquinone] 1 alpha subcomplex subunit 10, mitochondrial	NDUAA_HUMAN	1.62
	21	Cytochrome c1, heme protein, mitochondrial	CY1_HUMAN	1.30
Structure	25	Cysteine and glycine-rich protein 3	CSRP3_HUMAN	25.64
	1	Collagen α-1(VI) chain	CO6A1_HUMAN	6.43
	7	Desmin	DESM_HUMAN	2.81
	6	Tubulin β-4B chain	TBB4B_HUMAN	2.25
	2	Myosin heavy chain-7	MYH7_HUMAN	1.72
Survival	3	Stress-70 protein, mitochondrial	GRP75_HUMAN	3.48
	24	Superoxide dismutase [Mn], mitochondrial	SODM_HUMAN	1.96
Others	4	Serum albumin	ALBU_HUMAN	3.38
	26	Myoglobin	MYG_HUMAN	3.15
	20	Four and a half LIM domains protein 2	FHL2_HUMAN	1.85
	27	Myoglobin	MYG_HUMAN	1.45

Proteins with increased levels of 4HNE modification detected in RV failure versus RV hypertrophy by 2-dimensional gel electrophoresis and Western blot were identified using mass spectrometry (n=1 per group). Twenty-seven proteins were increased in RV failure versus RV hypertrophy with 100% protein score CIs for all proteins (>95% is considered significant). Fold change represents the increase in RV failure versus RV hypertrophy. 4HNE indicates 4-hydroxynonenal; NADH, nicotinamide adenine dinucleotide; and RV, right ventricle.

higher oxidative phosphorylation in moderate RV hypertrophy compared to RV failure. We also performed multiple regression analysis to understand the relationship between oxidative phosphorylation, patient's age, and disease categories (mild/moderate/severe RV hypertrophy and RV failure). Age was not independently associated with oxidative phosphorylation (–2.1[95% CI, –5.14 to 0.91]; P=0.158), while moderate hypertrophy was independently associated with oxidative phosphorylation (132.8 [95% CI, 69.14–196.4]; P=0.0004). The model was able to account for 70% of the variance in oxidative phosphorylation (R^2=0.6986; P=0.0004).

Mitochondrial Mass Is Not Decreased in RV Hypertrophy and RV Failure

We investigated whether mitochondrial mass decreased in RV failure thereby leading to a decrease in oxidative phosphorylation. Mitochondrial mass (measured by VDAC1 expression) and biogenesis (measured by PGC1α expression) were not decreased but actually trended toward being increased in RV failure (Figure 3A through 3C). As further evidence of maintained to increased mitochondrial biogenesis, mitochondrial DNA (mtDNA) was also assessed. mtDNA was not depleted as previously described for RV hypertrophy and

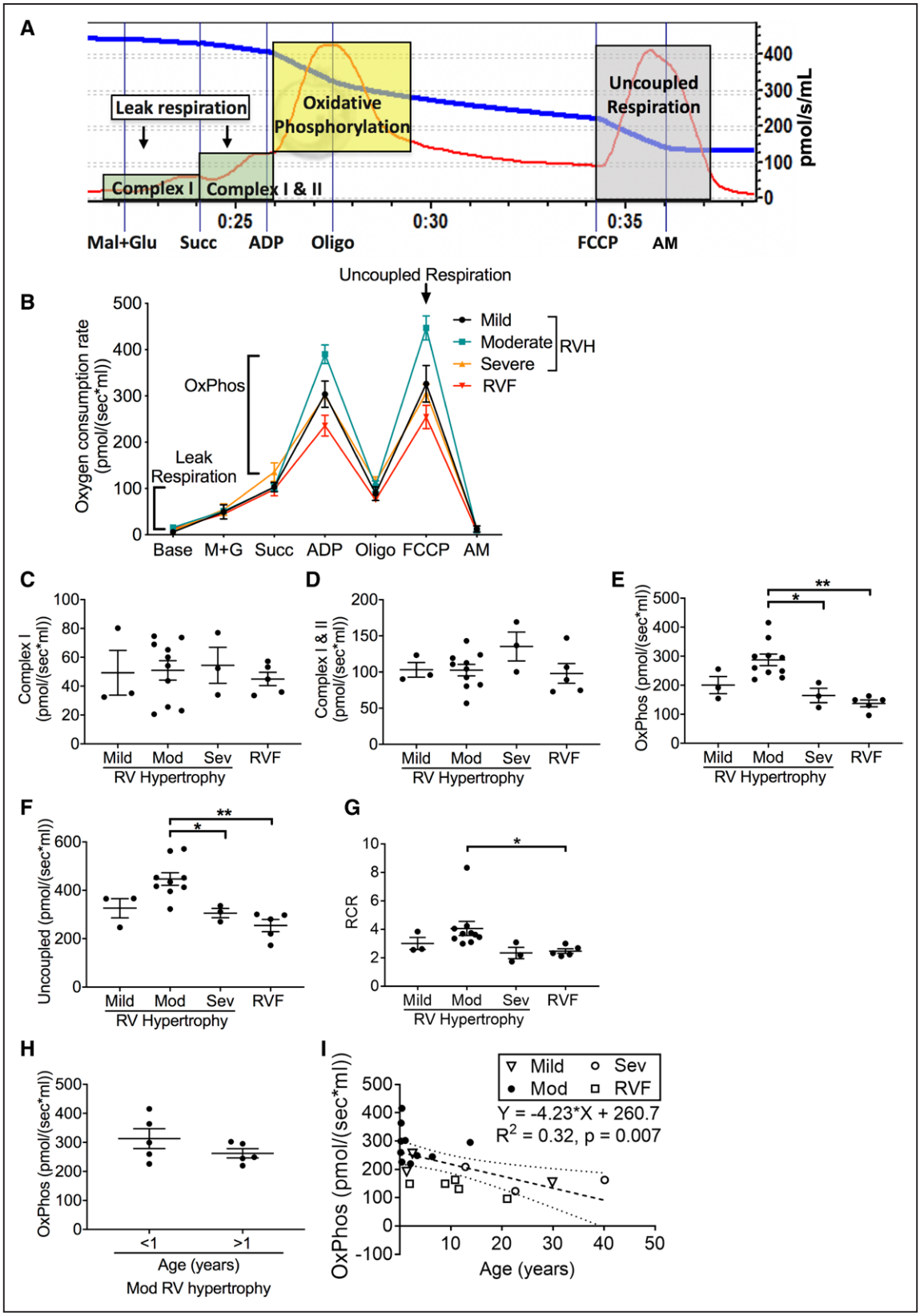

Figure 2. Patients with severe RV hypertrophy and RV failure demonstrate decreased oxidative phosphorylation.
A, A representative oxygen consumption tracing is shown for myocardial tissue (red curve) along with the available oxygen in the assay chamber (blue curve). We evaluated leak respiration (green shaded zones), oxidative phosphorylation (yellow shaded zone), and uncoupled respiration (gray shaded zone). **B,** Summary of oxygen consumption in right ventricular myocardial tissue (n=3–10 per group). **C, D,** Complex I– and Complex II–mediated oxygen consumption was unchanged across all groups. **E, F,** Oxidative phosphorylation and uncoupled respiration trended toward an increase from mild to moderate RV hypertrophy, decreased from moderate RV hypertrophy to severe hypertrophy, and decreased with RV failure. Oxidative phosphorylation remained significantly (*Continued*)

Figure 2 Continued. decreased after adjusting for age (*P*=0.0004) in RV failure. **G,** Similarly, respiratory control ratio trended toward an increase in moderate hypertrophy and subsequently significantly decreased from moderate RV hypertrophy to RV failure. **H,** Oxidative phosphorylation did not differ in patients with moderate RV hypertrophy between those <1 year of age versus >1 year of age (n=5 per group). **I,** Linear regression analysis demonstrates that age plays a role in the changes seen in oxidative phosphorylation, but the actual change in oxidative phosphorylation per year (slope) is small at −4.23pmol/sec×mL (n=21). AM indicates antimycin A; FCCP, carbonyl cyanide-p-trifluoromethoxyphenylhydrazone; M+G, malate and glutamate; Mod, moderate; Oligo, oligomycin; OxPhos, oxidative phosphorylation; RCR, respiratory control ratio. RV, right ventricle; RVF, right ventricular failure; Sev, severe; and Succ, succinate. Data are presented as mean±SEM. **P*<0.05, ***P*<0.01.

RV failure,[19] but instead was increased with RV failure (moderate RV hypertrophy, 356.5±28.85 vs RV failure, 960±180.6; *P*=0.025) (Figure 3D). mtDNA copy number was very variable in patients with RV failure.

RV Failure Is Characterized by Abnormal Mitochondrial Morphology and Disruption in Network Connectivity

We next assessed mitochondrial structure in RV failure using transmission electron microscopy. Severe RV hypertrophy samples were not available for transmission electron microscopy. Mitochondria were divided into 0.1 μm^2 size bins and a histogram was developed to evaluate mitochondrial size distribution (Figure 3E). Substantial heterogeneity was noted in mitochondrial size in all groups, however the size distribution and median mitochondrial size (Figure 3F) was not different between groups. Qualitatively, mitochondria lost their elongated shape and became more circular in moderate RV hypertrophy and more irregularly shaped in RV failure with decrease in cristae density and loss of network connectivity (Figure 3G). Substantial heterogeneity was also noted in mitochondrial dynamics proteins; however, the expression of fission protein DRP1 trended toward an increase and fusion protein MFN2 increased in RV failure (see Results and Figure II in the Data Supplement).

4HNE Treatment Attenuates Oxidative Phosphorylation-Mediated ATP Synthesis

Having shown an association between increased 4HNE adduction of mitochondrial enzymes, impaired oxidative phosphorylation, and mitochondrial structural changes, we next evaluated whether treatment with 4HNE can directly impair oxidative phosphorylation using HL1 cardiomyocytes and confirmed important changes in human induced pluripotent stem cell-derived cardiomyocytes. We first tested whether the systemic inotropic medications used in the RV failure patients such as the β adrenoreceptor agonist epinephrine could have caused the increase in 4HNE adduction. Commonly used in vitro β adrenoreceptor agonists norepinephrine and isoproterenol were used to treat HL1 cells and did not increase 4HNE expression (Figure IIIA and IIIB in the Data Supplement).

4HNE treatment resulted in increased formation of multiple 4HNE protein adducts similar to those seen in patients (Figure 4A and 4B) and decreased cell count (Figure 4C). To better evaluate which proteins underwent 4HNE-adduction, proteins with increased 4HNE-adduction were detected in 4HNE treated HL1 cardiomyocytes by 2-dimensional gel electrophoresis and Western blot and then identified using mass spectrometry and compared with control (Figure IVA and IVB). Fifteen 4HNE adducted proteins which increased in 4HNE treated cells (≥1.6-fold change) were selected for identification (Table III in the Data Supplement). Interestingly, 6 of the 15 proteins were metabolic pathway proteins and most were directly related to mitochondrial metabolism similar to that seen in patient RV failure including proteins involved in electron transport chain activity and mitochondrial respiration such as nicotinamide adenine dinucleotide dehydrogenase, cytochrome b, and cytochrome c. In addition, mitochondrial proteins involved in survival and stress response were targeted by 4HNE similar to that seen in patient RV failure. 4HNE adduction to proteins involved in mitochondrial respiration was associated with decreased oxygen consumption (Figure 4D through 4H). Of note, 4HNE decreased respiratory control ratio (control, 3.383±0.0565 vs 50 μmol/L 4HNE, 2.783±0.0766; *P*<0.0057) despite increased mitochondrial membrane potential, indicating that 4HNE attenuates oxidative phosphorylation by inhibiting the electron transport chain activity rather than by an increase in mitochondrial membrane leakage (Figure 4I and 4K). The effect of 4HNE on mitochondrial respiration was confirmed in human induced pluripotent stem cell-derived cardiomyocytes (Figure VA through VD in the Data Supplement). Similar to HL-1 cells, 4HNE decreased oxygen consumption and respiratory control ratio in human induced pluripotent stem cell-derived cardiomyocytes (Figure VE and VF in the Data Supplement).

Carvedilol Does Not Rescue 4HNE-Mediated Attenuation of ATP Synthesis

We next evaluated whether treatment with carvedilol can rescue 4HNE-mediated impairment of oxidative phosphorylation in HL1 cardiomyocytes since carvedilol is a knownn antioxidant, decreasing lipid peroxidation and 4HNE in ischemic and dilated cardiomyopathy.[13,14] Carvedilol decreased 4HNE protein adducts but did not improve oxygen consumption to baseline levels. However, mass spectrometry identified proteins involved in electron transport chain activity and mitochondrial

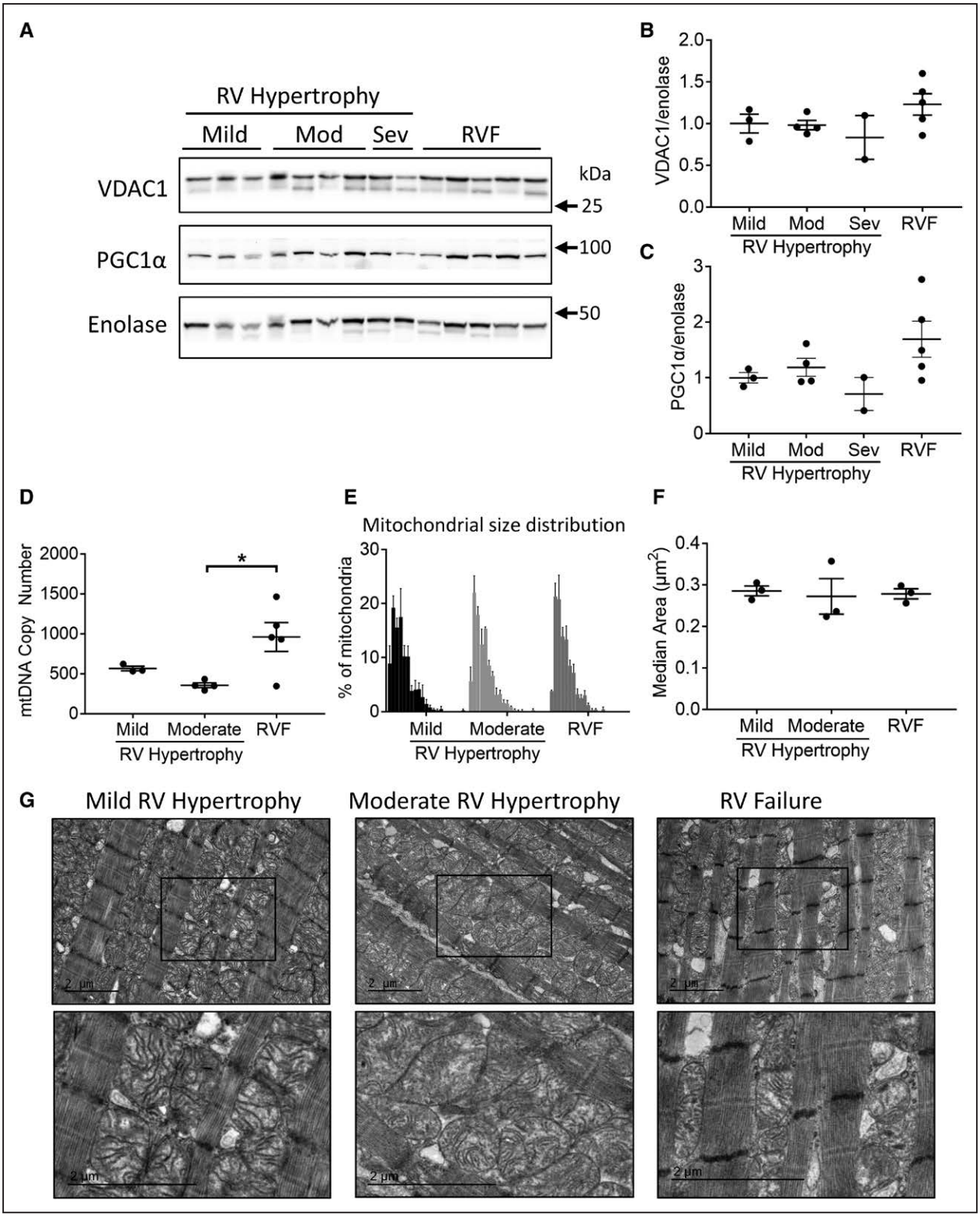

Figure 3. Patients with RV failure demonstrate mitochondrial structural changes.
A through **C,** Both VDAC1 (mitochondrial protein) and PGC1α (mitochondrial biogenesis factor) trended toward an increase in RV failure (n=2–5 per group). **D,** Mitochondrial DNA copy number was not different between mild and moderate RV hypertrophy groups, but was significantly increased from moderate RV hypertrophy to RV failure (n=3–5 per group). **E,** Histogram of mitochondrial size distribution for each group by transmission electron microscopy demonstrates no difference in mitochondrial size. Each bin represents increments in mitochondrial area of 0.1 μm^2 from left to right. Range= 0 to 2 μm^2. **F**, No significant difference was observed in median mitochondrial area. **G,** Representative transmission electron microscopy images. Mitochondria become more rounded in moderate RV hypertrophy and more irregular in shape in RV failure, with a loss of defined cristae structure. Scale bars are 2 μm. n=3 per group. Mod indicates moderate; mtDNA, mitochondrial DNA; RV, right ventricle; RVF, right ventricular failure; Sev, severe; and VDAC1, voltage-dependent anion-selective channel protein 1. Data are presented as mean±SEM. *P<0.05.

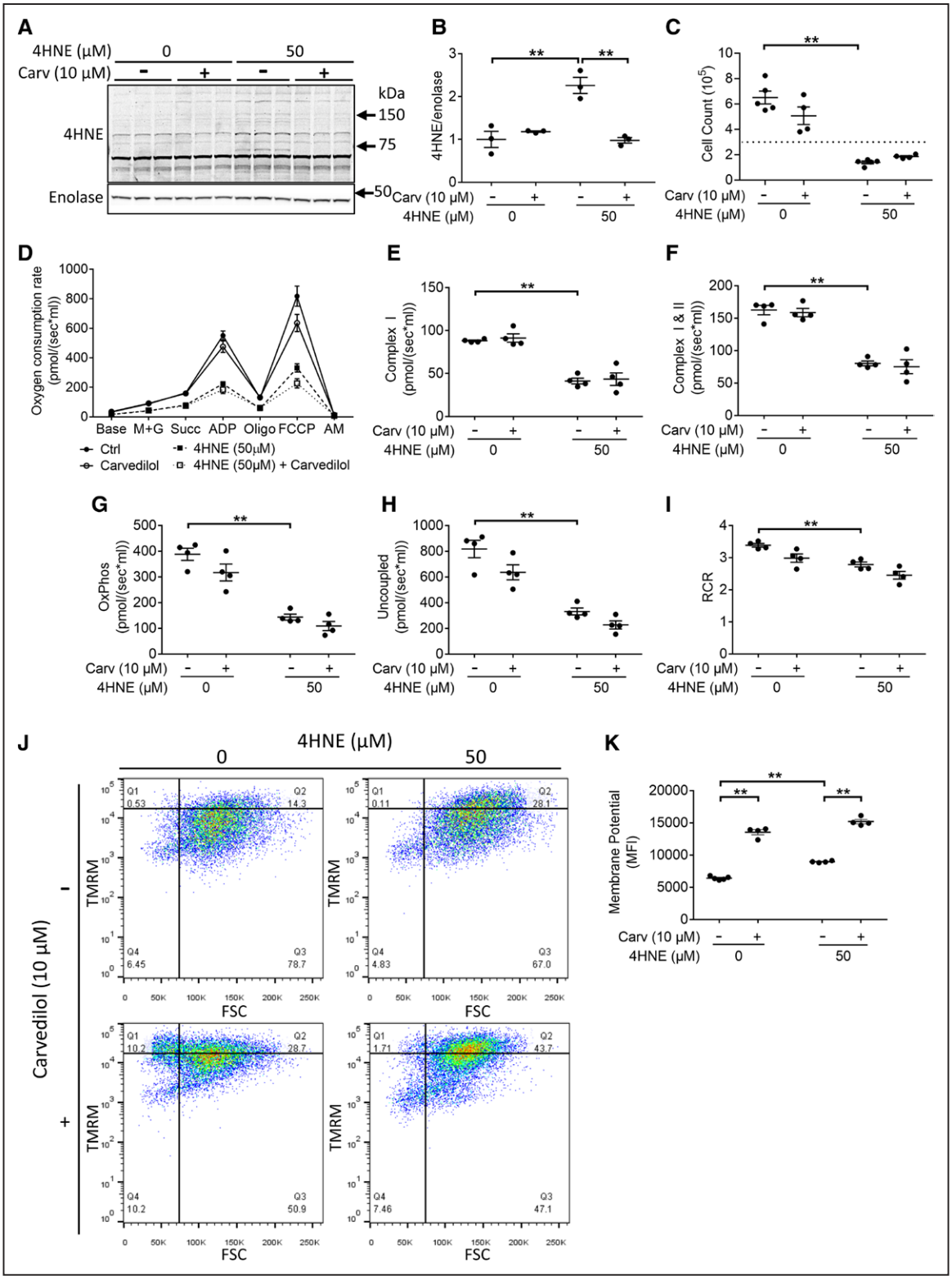

Figure 4. 4HNE treatment decreases ATP synthesis but increases mitochondrial membrane potential.
HL1 Cardiomyocytes were treated with 50 μM 4HNE for 24 hours and rescue was assessed with 10 μM carvedilol. **A, B**, 4HNE adducts increased after 4HNE treatment. Carvedilol decreased 4HNE adducts (n=3 per group). **C,** 4HNE decreased cell count—the horizontal dotted line denotes the original number of plated cells (n=4–5 per group). **D** through **I,** Oxygen consumption was assessed in response to 4HNE using high resolution respirometry. **D,** Summary of the oxygen consumption data. 4HNE decreased (**E, F**) leak respiration, (**G**) oxidative phosphorylation, (**H**) uncoupled respiration, and (**I**) respiratory control ratio (n=4 per group). **J, K,** However, 4HNE increased mitochondrial membrane potential, which further increased with carvedilol treatment (n=4–5 per group). 4HNE indicates 4-hydroxynonenal; AM, antimycin; Carv, carvedilol; FCCP, carbonyl cyanide 4-(trifluoromethoxy) phenylhydrazone; FSC, forward scatter; M+G, malate and glutamate; MFI, median fluorescence intensity; RCR, respiratory control ratio; Oligo, oligomycin; OxPhos, oxidative phosphorylation; Succ, succinate; and TMRM, tetramethylrhodamine, methyl ester. Data are presented as mean±SEM. $^{**}P<0.01$.

respiration such as nicotinamide adenine dinucleotide dehydrogenase, cytochrome b, and cytochrome c to be highly adducted to 4HNE despite carvedilol treatment, similar to that seen with 4HNE alone (Table III in the Data Supplement). This may explain the lack of improvement in oxygen consumption. Although carvedilol also increased the mitochondrial membrane potential, this is likely to be spurious based on the observation that leak respiration did not decrease concomitantly with the carvedilol-mediated increase in mitochondrial membrane potential. This may be detecting the deprotonated, negatively charged form of carvedilol in the high pH matrix environment,[20,21] rather than change in the hydrogen ion concentration gradient (Figure VI in the Data Supplement).

4HNE Increased Mitochondrial Mass and Alters Mitochondrial Structure

4HNE increased mitochondrial mass in HL1 cells by MitoTracker Red CMXRos fluorescence: control, 4212±306.9 versus 4HNE, 9817±212.4; $P<0.0001$ (Figure 5A and 5B) and VDAC1 expression: control, 1±0.03 versus 4HNE, 2.13±0.04; $P<0.0001$ (Figure 5C and 5D), even though it did not affect mitochondrial biogenesis

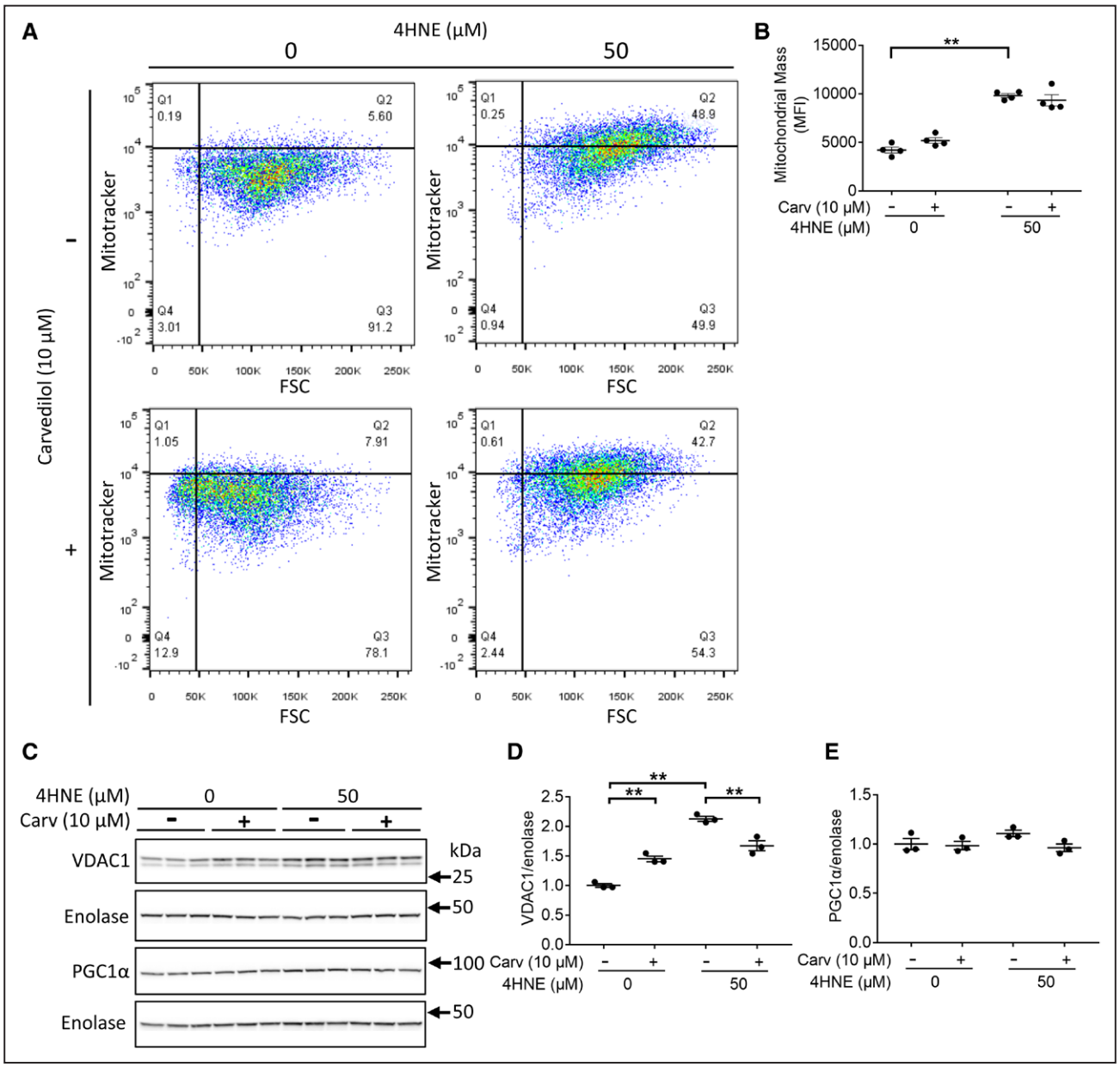

Figure 5. 4HNE treatment increases mitochondrial mass.
HL1 Cardiomyocytes were treated with 50 μM 4HNE and/or 10 μM carvedilol. **A, B,** 4HNE increased flow cytometric signal of Mitotracker Red CMXRos, a measure of mitochondrial mass (n=4 per group). **C, D,** 4HNE increased VDAC1 expression, another marker of mitochondrial mass, but this was inhibited by carvedilol. **E,** 4HNE did not decrease PGC1α expression, a marker of mitochondrial biogenesis (n=3 per group). 4HNE indicates 4-hydroxynonenal; Carv, carvedilol; FSC, forward scatter; and VDAC1, voltage-dependent anion-selective channel protein 1. Data are presented as mean±SEM. **$P<0.01$.

as indicated by unchanged PGC1α expression (Figure 5E). Fluorescence microscopy demonstrated no change in mitochondrial area with 4HNE (Figure 6A through 6C). However, 4HNE decreased mitochondrial perimeter (Figure 6D) and increased mitochondrial circularity, making them more compact and increased solidity leading to less surface ruffling (Figure 6E and 6F). Carvedilol did not change mitochondrial morphology. 4HNE treatment increased the whole-cell expression of fission proteins (Figure VIIA through VIIG). In contrast, despite whole-cell level increase in fission proteins, mitochondrial localization of the fission and fusion proteins were inhibited by 4HNE (Figure VIIH through VIIN and Results in the Data Supplement).

DISCUSSION

For many children with congenital heart disease or pulmonary hypertension, pressure overload stress on the RV exists throughout life, even after successful surgical repair or palliation leading to RV hypertrophy and dilation and eventually RV failure.[3,22] We focused on the dysregulation of myocardial energy generation as a driver for the development of RV failure in children with congenital heart disease with RV pressure overload. We show that RV failure is characterized by increased 4HNE adduction of metabolic and mitochondrial proteins. This was associated with decreased myocardial energy generation and mitochondrial structural disruption with increasing severity of RV hypertrophy and RV failure. Mechanistically, we show that 4HNE is sufficient to decrease energy generation by inhibiting electron transport chain complex activities and mitochondrial dynamics.

Increased oxidative stress has been shown in RV pressure overload because of pulmonary hypertension[23,24] and in left ventricular hypertrophy,[25] but no data exists on the posttranslational modification of mitochondrial enzymes by 4HNE and its effects in RV hypertrophy and failure. We show that whereas all patients with RV failure demonstrate increased lipid peroxidation, there is significant interpatient variability. We speculate that the duration and severity of heart failure, as well as the use of systemic inotropic agents, can influence the degree of oxidative stress.[26,27] 4HNE-induced oxidative stress has previously been recognized in the left ventricle with ischemic heart disease because of myocardial infarction,[28] doxorubicin cardiotoxicity,[29] and dilated cardiomyopathy.[14] Cardiomyocyte mitochondria can be damaged not only by the 4HNE generated locally, but also by exogenous 4HNE,[30] such as circulating 4HNE seen in heart failure patients.[31] Zhao et al identified several 4HNE-adducted mitochondrial proteins in a preclinical murine model of doxorubicin cardiotoxicity and demonstrated decreased activity of the electron transport chain.[10,11,32] We show, for the first time, an increase in 4HNE adduction preferentially targeting metabolic and mitochondrial proteins in the myocardium in pressure overload-induced RV failure in children with congenital heart disease. 4HNE-mediated damage in the failing RV not only decreases electron transport chain activity, thereby generating less energy, but also adducts to sarcomeric proteins, cytoskeletal proteins, and prosurvival proteins, all of which may work in concert leading to a heart failure phenotype. This data provides valuable insight into the pathological changes in the RV that may trigger and/or exacerbate RV failure.

We show that although moderate RV hypertrophy demonstrates a trend toward a potential compensatory upregulation of mitochondrial energy generation, this is lost with increasing severity of RV hypertrophy, which may be a precursor to the development of RV failure. The decrease in oxidative phosphorylation occurs despite preserved mitochondrial mass and despite increased cardiac workload with hypertrophy and heart failure. The decrease in oxidative phosphorylation could serve as a marker for the need for earlier intervention to relieve RV pressure overload and preserve long-term RV function. The decrease in oxygen consumption seen in severe hypertrophy could also be related to the longer duration of hypertrophy, suggesting that sustained cardiac hypertrophy may cause a dysfunctional mitochondrial phenotype similar to that seen in cardiac aging. This is comparable to work by Karamanlidis et al[19] showing preserved mitochondrial activity in RV hypertrophy with preserved RV function and impaired mitochondrial activity in children with RV failure. However, while Karamanlidis et al indirectly measured mitochondrial activity by citrate synthase and succinate dehydrogenase activities, we show a direct high-resolution measurement of mitochondrial respiration as a function of both electron transport chain complex activities (rates of proton gradient generation and electron transfer) and mitochondrial membrane integrity (proton leak).

Lipid peroxidation is also known to damage mitochondrial DNA,[33,34] which is essential for mitochondrial biogenesis.[35,36] The increase in mitochondrial DNA copy number seen in RV failure may be related to the oxidative stress-induced upregulation of mitochondrial DNA synthesis.[37] This differs from that reported by Karamanlidis et al,[19] who demonstrated a progressive decrease in mitochondrial biogenesis in children with RV pressure overload from hypertrophy to failure. The differences seen in our study may be related to the different group of patients with RV failure, namely single ventricle in their study and a biventricular circulation in ours, and to the high levels of lipid peroxidation seen in our patients. Furthermore, the difference in patient ages may be a confounding factor. Whereas the RV failure patients studied by Karamanlidis et al were very young (range, 0.1–1.5 years), the average age of our RV failure patients was 10.9±6.9 years.

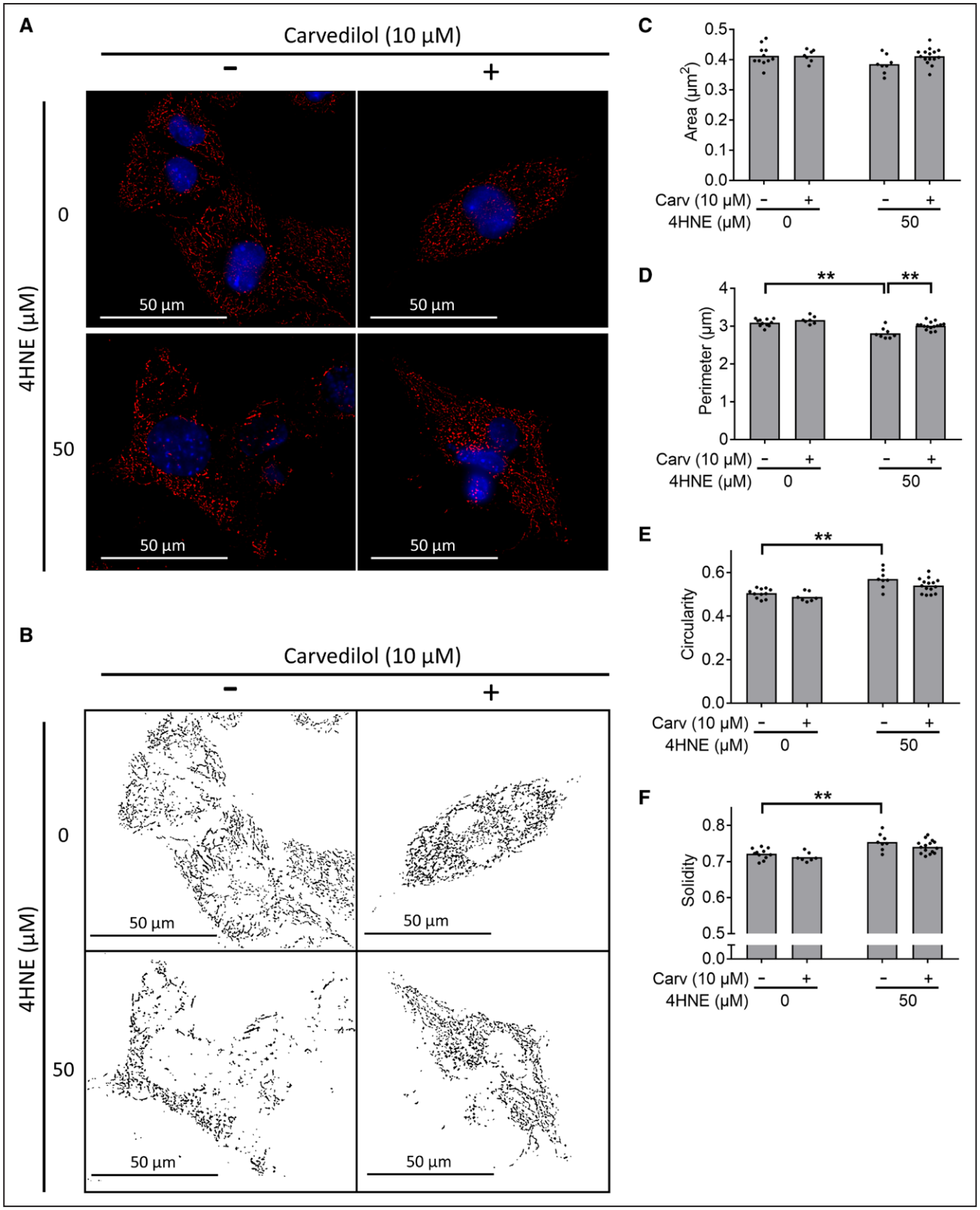

Figure 6. 4HNE decreases mitochondrial network connectivity.
Cardiomyocytes were stained with Mitotracker Red CMXRos (red) and Hoechst 33342 (blue) for mitochondrial and nuclear staining, respectively. Treatment with 50 μM 4HNE for 24 hours (**A, B**) disrupted mitochondrial network connectivity and Carvedilol improved network connectivity, did not demonstrate a change in mitochondrial area (**C**), decreased perimeter (**D**), and increased circularity and solidity (**E** and **F**). Scale bars are 50 μm. 4HNE indicates 4-hydroxynonenal. Data are presented as mean±SEM. $^{**}P<0.01$.

Mechanistically, we show the direct effects of 4HNE on cardiomyocyte energy generation to implicate its role in the development of RV failure, where 4HNE decreases oxygen consumption by inhibiting the electron transport chain complexes and inhibiting fission and fusion. In pathological patient brain and plasma, 4HNE concentrations can increase to between 1 and 10 μM, and in some cases, even up to 100 μM.[38,39] As such, in vivo cardiomyocyte mitochondria can be damaged not only by the 4HNE generated locally but also by exogenous 4HNE,[30] such as circulating 4HNE seen in heart failure patients.[31] Of note, although the concentration of 4HNE we have used in our study (50 μM) is still physiologically relevant, it exceeds the typically observed in vivo 4HNE levels. However, with this high concentration, we were able to show that 4HNE has acute dysregulatory effects on the mitochondrial function. It is interesting that among these effects, 4HNE also increased mitochondrial mass. This is consistent with previously reported findings that knockout of both fission and fusion proteins in the heart leads to increased mitochondrial mass.[40] 4HNE-induced mitochondrial membrane hyperpolarization[41–43] can further exacerbate lipid peroxidation, mitochondrial damage, and cell death, all of which have previously been shown in end stage ischemic heart failure in adults.[44] Our in vitro model does not fully recapitulate the human heart failure phenotype because of the lack of various in vivo stressors such as pressure overload and hypoxia. However, it provides insight into the effect of exogenous 4HNE on cardiomyocyte function.

Our data provide a rationale for developing drugs to mitigate lipid peroxidative damages. Carvedilol is one of the mainstays in clinical heart failure therapy and has shown promise in pulmonary hypertension induced RV failure.[45] While the ability of carvedilol to reduce lipid peroxidation has been reported,[14,46–48] it is not known whether it can also confer protection against reactive lipid peroxidation products. Carvedilol inhibited overall 4HNE adduction, but many mitochondrial and metabolic proteins remained adducted to 4HNE; thus, while carvedilol has antioxidant properties, it was unable to rescue 4HNE-mediated decrease in mitochondrial energy generation. However, under basal conditions, carvedilol leads to a favorable mitochondrial phenotype by decreasing fission, increasing fusion, increasing mitochondrial mass, and improving mitochondrial membrane potential, suggesting that this may still be beneficial in patients at risk for the development of heart failure.

CONCLUSION

Metabolic, mitochondrial, and key sarcomeric and cytoskeletal proteins are susceptible to 4HNE-adduction in RV failure. This is associated with impaired mitochondrial energy generation even in severe RV hypertrophy before the development of RV dysfunction and RV failure in patients with RV pressure overload. Mechanistically, we show that 4HNE impairs myocardial energy generation by inhibiting electron transport chain complexes and inhibiting mitochondrial dynamics. Carvedilol could not rescue the 4HNE-mediated impairment in energy generation. Strategies to decrease lipid peroxidation may improve myocardial energy generation and thereby preserve long-term heart function in patients with congenital heart disease. As surgical techniques for repair of complex congenital heart lesions continue to improve, long-term survival and quality of life will increasingly depend on our ability to preserve long-term RV function.

ARTICLE INFORMATION

Received May 8, 2020; accepted July 23, 2020.

The Data Supplement is available with this article at https://www.ahajournals.org/doi/suppl/10.1161/circulationaha.120.045470.

Correspondence

Sushma Reddy, 750 Welch Road, Suite 305, Stanford University, Palo Alto, CA 94305. Email sureddy@stanford.edu

Affiliations

Department of Pediatrics (Cardiology) (HT.V.H., N.S., S.L.P., S. Ranjbarvairi, D-Q.H., M.Z., G.F., D.B., S. Reddy), Department of Bioengineering (I.S.L.), and Department of Medicine (Cardiology) (S.M.W.), Stanford University, Palo Alto, CA. Department of Biology, Whitman College, Walla Walla, WA (M.C.). Department of Medicine, University of Washington, Seattle (K.B.K.).

Acknowledgments

The authors are solely responsible for the contents of the article, which do not necessarily represent the official views of the National Center for Research Resources or the National Institutes of Health. The authors thank the human subjects research coordinators, Sara Sherman-Levine and Aihua Zhu, who were supported by National Institutes of Health/National Center for Advancing Translational Sciences/Clinical and Translational Science Awards grant UL1 TR001085, the Lucile Packard Foundation for Children's Health, and the Child Health Research Institute. The authors thank Helen Lu for the analysis of the EM data and Julia Ryan for technical assistance with iPSC maintenance and cardiac differentiation. The authors thank the pediatric congenital cardiac surgeons, Drs Frank Hanley, Mohan Reddy, Katsuhide Meada, and Michael Ma, the surgical physician assistant team, and the operating room nursing staff for the patient myocardial samples.

Sources of Funding

The JEOL JEM1400 electron microscope at the Cell Sciences Imaging Facility of Stanford University was funded by a National Institutes of Health Shared Instrumentation grant (William Talbot, principal investigator; installation date, January 2011) and the American Recovery and Reinvestment Act award 1S10RR026780-01 from the National Center for Research Resources. This work is supported by grants from the National Institutes of Health (K08 HL127277-01 NIH to S.R. and K08HL148553 to S.L.P.); Reddy Foundation (to S.R.); and Department of Defense (PR151448 to D.B. and S.R.).

Disclosures

None.

REFERENCES

1. Altmann K, Printz BF, Solowiejczky DE, Gersony WM, Quaegebeur J, Apfel HD. Two-dimensional echocardiographic assessment of right ventricular

function as a predictor of outcome in hypoplastic left heart syndrome. *Am J Cardiol.* 2000;86:964–968. doi: 10.1016/s0002-9149(00)01131-0
2. Bogaard HJ, Abe K, Vonk Noordegraaf A, Voelkel NF. The right ventricle under pressure: cellular and molecular mechanisms of right-heart failure in pulmonary hypertension. *Chest.* 2009;135:794–804. doi: 10.1378/chest.08-0492
3. Fine NM, Chen L, Bastiansen PM, Frantz RP, Pellikka PA, Oh JK, Kane GC. Outcome prediction by quantitative right ventricular function assessment in 575 subjects evaluated for pulmonary hypertension. *Circ Cardiovasc Imaging.* 2013;6:711–721. doi: 10.1161/CIRCIMAGING.113.000640
4. Haddad F, Hunt SA, Rosenthal DN, Murphy DJ. Right ventricular function in cardiovascular disease, part I: anatomy, physiology, aging, and functional assessment of the right ventricle. *Circulation.* 2008;117:1436–1448. doi: 10.1161/CIRCULATIONAHA.107.653576
5. Reddy S, Bernstein D, Newburger JW. Renin-angiotensin-aldosterone system inhibitors for right ventricular dysfunction in tetralogy of Fallot: quo vadis? *Circulation.* 2018;137:1472–1474. doi: 10.1161/CIRCULATIONAHA.117.032285
6. Weiss RG, Gerstenblith G, Bottomley PA. ATP flux through creatine kinase in the normal, stressed, and failing human heart. *Proc Natl Acad Sci U S A.* 2005;102:808–813. doi: 10.1073/pnas.0408962102
7. Ide T, Tsutsui H, Kinugawa S, Utsumi H, Kang D, Hattori N, Uchida K, Arimura Ki, Egashira K, Takeshita A. Mitochondrial electron transport complex I is a potential source of oxygen free radicals in the failing myocardium. *Circ Res.* 1999;85:357–363. doi: 10.1161/01.res.85.4.357
8. Srivastava S, Chandrasekar B, Bhatnagar A, Prabhu SD. Lipid peroxidation-derived aldehydes and oxidative stress in the failing heart: role of aldose reductase. *Am J Physiol Heart Circ Physiol.* 2002;283:H2612–H2619. doi: 10.1152/ajpheart.00592.2002
9. Lucas DT, Szweda LI. Cardiac reperfusion injury: aging, lipid peroxidation, and mitochondrial dysfunction. *Proc Natl Acad Sci U S A.* 1998;95:510-514. doi: 10.1073/pnas.95.2.510
10. Chen J, Schenker S, Frosto TA, Henderson GI. Inhibition of cytochrome c oxidase activity by 4-hydroxynonenal (HNE). Role of HNE adduct formation with the enzyme subunits. *Biochim Biophys Acta.* 1998;1380:336–344. doi: 10.1016/s0304-4165(98)00002-6
11. Petersen DR, Doorn JA. Reactions of 4-hydroxynonenal with proteins and cellular targets. *Free Radic Biol Med.* 2004;37:937–945. doi: 10.1016/j.freeradbiomed.2004.06.012
12. Anderson EJ, Katunga LA, Willis MS. Mitochondria as a source and target of lipid peroxidation products in healthy and diseased heart. *Clin Exp Pharmacol Physiol.* 2012;39:179–193. doi: 10.1111/j.1440-1681.2011.05641.x
13. Moreno AJ, Santos DJ, Palmeira CM. Ischemic heart disease: the role of mitochondria–carvedilol prevents lipid peroxidation of mitochondrial membranes. *Rev Port Cardiol.* 1998;17 Suppl 2:Ii63-77.
14. Nakamura K, Kusano K, Nakamura Y, Kakishita M, Ohta K, Nagase S, Yamamoto M, Miyaji K, Saito H, Morita H, et al. Carvedilol decreases elevated oxidative stress in human failing myocardium. *Circulation.* 2002;105:2867–2871. doi: 10.1161/01.cir.0000018605.14470.dd
15. Cordero-Reyes AM, Gupte AA, Youker KA, Loebe M, Hsueh WA, Torre-Amione G, Taegtmeyer H, Hamilton DJ. Freshly isolated mitochondria from failing human hearts exhibit preserved respiratory function. *J Mol Cell Cardiol.* 2014;68:98–105. doi: 10.1016/j.yjmcc.2013.12.029
16. Nowak G, Bakajsova D, Clifton GL. Protein kinase C-epsilon modulates mitochondrial function and active Na+ transport after oxidant injury in renal cells. *Am J Physiol Renal Physiol.* 2004;286:F307–F316. doi: 10.1152/ajprenal.00275.2003
17. Jastroch M, Divakaruni AS, Mookerjee S, Treberg JR, Brand MD. Mitochondrial proton and electron leaks. *Essays Biochem.* 2010;47:53–67. doi: 10.1042/bse0470053
18. Schindelin J, Arganda-Carreras I, Frise E, Kaynig V, Longair M, Pietzsch T, Preibisch S, Rueden C, Saalfeld S, Schmid B, et al. Fiji: an open-source platform for biological-image analysis. *Nat Methods.* 2012;9:676–682. doi: 10.1038/nmeth.2019
19. Karamanlidis G, Bautista-Hernandez V, Fynn-Thompson F, Del Nido P, Tian R. Impaired mitochondrial biogenesis precedes heart failure in right ventricular hypertrophy in congenital heart disease. *Circ Heart Fail.* 2011;4:707–713. doi: 10.1161/CIRCHEARTFAILURE.111.961474
20. Oliveira PJ, Marques MP, Batista de Carvalho LA, Moreno AJ. Effects of carvedilol on isolated heart mitochondria: evidence for a protonophoretic mechanism. *Biochem Biophys Res Commun.* 2000;276:82–87. doi: 10.1006/bbrc.2000.3374
21. Soleymanpour A, Ghasemian M. Chemically modified carbon paste sensor for the potentiometric determination of carvedilol in pharmaceutical and biological media. *Measurement.* 2015;59:14-20.
22. Therrien J, Siu SC, McLaughlin PR, Liu PP, Williams WG, Webb GD. Pulmonary valve replacement in adults late after repair of tetralogy of Fallot: are we operating too late? *J Am Coll Cardiol.* 2000;36:1670–1675. doi: 10.1016/s0735-1097(00)00930-x
23. Pichardo J, Palace V, Farahmand F, Singal PK. Myocardial oxidative stress changes during compensated right heart failure in rats. *Mol Cell Biochem.* 1999;196:51–57.
24. Redout EM, van der Toorn A, Zuidwijk MJ, van de Kolk CW, van Echteld CJ, Musters RJ, van Hardeveld C, Paulus WJ, Simonides WS. Antioxidant treatment attenuates pulmonary arterial hypertension-induced heart failure. *Am J Physiol Heart Circ Physiol.* 2010;298:H1038–H1047. doi: 10.1152/ajpheart.00097.2009
25. Dolinsky VW, Chan AY, Robillard Frayne I, Light PE, Des Rosiers C, Dyck JR. Resveratrol prevents the prohypertrophic effects of oxidative stress on LKB1. *Circulation.* 2009;119:1643–1652. doi: 10.1161/CIRCULATIONAHA.108.787440
26. Rathore N, John S, Kale M, Bhatnagar D. Lipid peroxidation and antioxidant enzymes in isoproterenol induced oxidative stress in rat tissues. *Pharmacol Res.* 1998;38:297–303. doi: 10.1006/phrs.1998.0365
27. Mari Kannan M and Darlin Quine S. Ellagic acid protects mitochondria from β-adrenergic agonist induced myocardial damage in rats; evidence from in vivo, in vitro and ultra structural study. *Food Res Int.* 2012;45:1-8.
28. Campos JC, Queliconi BB, Dourado PM, Cunha TF, Zambelli VO, Bechara LR, Kowaltowski AJ, Brum PC, Mochly-Rosen D, Ferreira JC. Exercise training restores cardiac protein quality control in heart failure. *PLoS One.* 2012;7:e52764. doi: 10.1371/journal.pone.0052764
29. Zhao Y, Miriyala S, Miao L, Mitov M, Schnell D, Dhar SK, Cai J, Klein JB, Sultana R, Butterfield DA, et al. Redox proteomic identification of HNE-bound mitochondrial proteins in cardiac tissues reveals a systemic effect on energy metabolism after doxorubicin treatment. *Free Radic Biol Med.* 2014;72:55–65. doi: 10.1016/j.freeradbiomed.2014.03.001
30. Hill BG, Dranka BP, Zou L, Chatham JC, Darley-Usmar VM. Importance of the bioenergetic reserve capacity in response to cardiomyocyte stress induced by 4-hydroxynonenal. *Biochem J.* 2009;424:99–107. doi: 10.1042/BJ20090934
31. Mak S, Lehotay DC, Yazdanpanah M, Azevedo ER, Liu PP, Newton GE. Unsaturated aldehydes including 4-OH-nonenal are elevated in patients with congestive heart failure. *J Card Fail.* 2000;6:108–114.
32. Xiao M, Zhong H, Xia L, Tao Y, Yin H. Pathophysiology of mitochondrial lipid oxidation: Role of 4-hydroxynonenal (4-HNE) and other bioactive lipids in mitochondria. *Free Radic Biol Med.* 2017;111:316–327. doi: 10.1016/j.freeradbiomed.2017.04.363
33. Almeida AM, Bertoncini CR, Borecký J, Souza-Pinto NC, Vercesi AE. Mitochondrial DNA damage associated with lipid peroxidation of the mitochondrial membrane induced by Fe2+-citrate. *An Acad Bras Cienc.* 2006;78:505–514. doi: 10.1590/s0001-37652006000300010
34. Hruszkewycz AM. Evidence for mitochondrial DNA damage by lipid peroxidation. *Biochem Biophys Res Commun.* 1988;153:191–197. doi: 10.1016/s0006-291x(88)81207-5
35. Chen L, Gong Q, Stice JP, Knowlton AA. Mitochondrial OPA1, apoptosis, and heart failure. *Cardiovasc Res.* 2009;84:91–99. doi: 10.1093/cvr/cvp181
36. Tian L, Neuber-Hess M, Mewburn J, Dasgupta A, Dunham-Snary K, Wu D, Chen KH, Hong Z, Sharp WW, Kutty S, et al. Ischemia-induced Drp1 and Fis1-mediated mitochondrial fission and right ventricular dysfunction in pulmonary hypertension. *J Mol Med (Berl).* 2017;95:381–393. doi: 10.1007/s00109-017-1522-8
37. Lee HC, Wei YH. Mitochondrial biogenesis and mitochondrial DNA maintenance of mammalian cells under oxidative stress. *Int J Biochem Cell Biol.* 2005;37:822–834. doi: 10.1016/j.biocel.2004.09.010
38. Dodson M, Wani WY, Redmann M, Benavides GA, Johnson MS, Ouyang X, Cofield SS, Mitra K, Darley-Usmar V, Zhang J. Regulation of autophagy, mitochondrial dynamics, and cellular bioenergetics by 4-hydroxynonenal in primary neurons. *Autophagy.* 2017;13:1828–1840. doi: 10.1080/15548627.2017.1356948
39. Strohmaier H, Hinghofer-Szalkay H, Schaur RJ. Detection of 4-hydroxynonenal (HNE) as a physiological component in human plasma. *J Lipid Mediat Cell Signal.* 1995;11:51–61. doi: 10.1016/0929-7855(94)00027-a
40. Song M, Franco A, Fleischer JA, Zhang L, Dorn GW II. Abrogating mitochondrial dynamics in mouse hearts accelerates mitochondrial senescence. *Cell Metab.* 2017;26:872–883.e5. doi: 10.1016/j.cmet.2017.09.023
41. Jheng HF, Tsai PJ, Guo SM, Kuo LH, Chang CS, Su IJ, Chang CR, Tsai YS. Mitochondrial fission contributes to mitochondrial dysfunction and insulin resistance in skeletal muscle. *Mol Cell Biol.* 2012;32:309–319. doi: 10.1128/MCB.05603-11

42. Disatnik MH, Ferreira JC, Campos JC, Gomes KS, Dourado PM, Qi X, Mochly-Rosen D. Acute inhibition of excessive mitochondrial fission after myocardial infarction prevents long-term cardiac dysfunction. *J Am Heart Assoc.* 2013;2:e000461. doi: 10.1161/JAHA.113.000461
43. Lee YJ, Jeong SY, Karbowski M, Smith CL, Youle RJ. Roles of the mammalian mitochondrial fission and fusion mediators Fis1, Drp1, and Opa1 in apoptosis. *Mol Biol Cell.* 2004;15:5001–5011. doi: 10.1091/mbc.e04-04-0294
44. Sabbah HN. Apoptotic cell death in heart failure. *Cardiovasc Res.* 2000;45:704–712. doi: 10.1016/s0008-6363(99)00348-x
45. Grinnan D, Bogaard HJ, Grizzard J, Van Tassell B, Abbate A, DeWilde C, Priday A, Voelkel NF. Treatment of group I pulmonary arterial hypertension with carvedilol is safe. *Am J Respir Crit Care Med.* 2014;189:1562–1564. doi: 10.1164/rccm.201311-2025LE
46. Huang H, Shan J, Pan XH, Wang HP, Qian LB, Xia Q. Carvedilol improved diabetic rat cardiac function depending on antioxidant ability. *Diabetes Res Clin Pract.* 2007;75:7–13. doi: 10.1016/j.diabres.2006.04.016
47. Kumar A, Dogra S, Prakash A. Effect of carvedilol on behavioral, mitochondrial dysfunction, and oxidative damage against D-galactose induced senescence in mice. *Naunyn Schmiedebergs Arch Pharmacol.* 2009;380:431–441. doi: 10.1007/s00210-009-0442-8
48. Sahu BD, Koneru M, Bijargi SR, Kota A, Sistla R. Chromium-induced nephrotoxicity and ameliorative effect of carvedilol in rats: Involvement of oxidative stress, apoptosis and inflammation. *Chem Biol Interact.* 2014;223:69–79. doi: 10.1016/j.cbi.2014.09.009
49. Burridge PW, Matsa E, Shukla P, Lin ZC, Churko JM, Ebert AD, Lan F, Diecke S, Huber B, Mordwinkin NM, et al. Chemically defined generation of human cardiomyocytes. *Nat Methods.* 2014;11:855–860. doi: 10.1038/nmeth.2999
50. Sharma A, Li G, Rajarajan K, Hamaguchi R, Burridge PW, Wu SM. Derivation of highly purified cardiomyocytes from human induced pluripotent stem cells using small molecule-modulated differentiation and subsequent glucose starvation. *J Vis Exp.* 2015:52628. doi: 10.3791/52628